Nonlinear Control for a Model-scaled Helicopter with Constraints on Rotor Thrust and Fuselage Attitude

ZHU Bing[1, 2, 3] HUO Wei[1, 3]

[1.] The Seventh Research Division, Beihang University, Beijing 100191, China
[2.] Department of Electrical, Electronic and Computer Engineering, University of Pretoria, Pretoria 0083, South Africa
[3.] Science and Technology on Aircraft Control Laboratory, Beihang University, Beijing 100191, China

Abstract A nonlinear control is proposed for trajectory track-ing of a 6-DOF model-scaled helicopter with constraints on main rotor thrust and fuselage attitude. In the procedure of con-trol design, the mathematical model of helicopter is simplified into three subsystems: altitude subsystem, longitudinal-lateral subsystem and attitude subsystem. The proposed control is developed by combining the sub-controls for the correspond-ing subsystems. The sub-controls for altitude subsystem and longitudinal-lateral subsystem are designed with hyperbolic tangent functions to satisfy the constraints; the sub-control for attitude subsystem is based on backstepping technique such that fuselage attitude tracks the virtual control for longitudinal-lateral subsystem. It is proved theoretically that tracking errors are ultimately bounded, and control constraints are satisfied. Performances of the proposed controller are demonstrated by simulation results.

Key words Nonlinear control, trajectory tracking, helicopter control, saturated control

Trajectory tracking control design for a 6-DOF autonomous model-scaled helicopter has becomes an interesting and challenging task in recent years, because of the nonlinearities and couplings in its dynamic model[1−2]. Some representative researches include linear control[3], approximate feedback linearization[2], backstepping[4−5], robust H_∞ control[6−7], composite nonlinear feedback[8], and model predictive control[9].

Traditionally, nonlinear trajectory tracking controls for helicopters are mainly based on some assumptions: 1) constant rotational rate of rotors, 2) simplified expressions for rotor thrusts in case of low fuselage velocity and acceleration, and 3) negligence of small coupling terms (or small body forces). To support the assumptions, however, some other significant issues require further consideration. The desired main rotor thrust should be subjected to saturation; otherwise, excessively large main rotor thrust would result in large acceleration of the fuselage, and the simplified expressions for rotor thrusts are unreasonable. Besides, large rotor thrust requires large collective pitch, increasing drag forces exerted on the rotor blades and deteriorating the assumption of constant rotational rate. Moreover, attitude of the fuselage should be bounded securely for the reason that aggressive attitude often leads to uncontrollability in case of constraint on rotor thrust.

Many early works on saturated control[10−13] presented the fundamental principles and applications. Saturated control for nonlinear systems was then developed and summarized[14−17]. Saturated control strategies were applied to some specific projects, such as 3-DOF VTOL aircraft[18−19], linear motor system[20], and inverted pendulum[21]. However, researches on saturated control for trajectory tracking of 6-DOF helicopter were relatively rare. Controllers for helicopters subject to input constraints were often designed partially saturated[4, 22−23] due to nonlinearities and couplings in mathematical modeling.

Generally, saturated control are designed by using non-smooth saturation functions, which impedes analytical solution for derivatives of virtual controls, and application of Barbalat lemma to stability analysis. To overcome the troubles resulted from non-smooth saturation functions, it is necessary to apply some smooth saturation functions. Recently, a smooth hyperbolic saturated control has been designed for a 3-DOF VTOL aircraft[18]; stability results of the closed-loop system were simple to prove, and the control algorithm was easy to implement.

Enlightened by the simple smooth saturated control for 3-DOF aircraft[18], we propose a nonlinear control based on smooth saturation function for a fully 6-DOF model-scaled helicopter under constraints of main rotor thrust and fuselage attitude. The constraints are addressed by using bounded and continuously differentiable hyperbolic tangent functions. The full nonlinear model of the helicopter plant is divided into three subsystems, and the proposed control is designed by combining the sub-controls developed for the corresponding subsystems. The main contributions of this paper include: 1) The result of a 3-DOF (lateral, altitude and roll) VTOL aircraft[18] is extended to a 6-DOF helicopter; 2) Exponential stability and local input-to-state stability (LISS)[24] of the smooth saturated control system are discussed in detail; 3) Neglected coupling terms are considered theoretically in the stability analysis of the closed-loop system; 4) Time derivatives of virtual controls are presented in explicit forms without using differentiators to reduce the amount of calculation significantly.

This paper is organized as following: some useful preliminaries are reviewed in Section 1; the problem of trajectory tracking for helicopter subject to constraint on main rotor thrust and fuselage attitude is formulated in Section 2; detailed control design procedure is proposed in Section 3; the stability concerning the closed-loop system with neglected terms is analyzed in Section 4; simulation results are presented in Section 5 to illustrate the performances of the designed controller; this paper is concluded in Section 6.

1 Theoretical preliminaries

Throughout this paper, $|\cdot|$ is defined as the absolute value for real numbers; $\|\cdot\|$ is defined as the Euclidean norm for vectors, and the induced Euclidean norm for matrices.

The conventional non-smooth saturation function is given by

$$\mathrm{sat}_\epsilon(x) = \begin{cases} x, & \text{if } |x| < \epsilon \\ \epsilon, & \text{if } |x| \geq \epsilon \end{cases}$$

which often brings the difficulties of 1) solving analytically the derivatives of the virtual control, and 2) applying Barbalat lemma to the stability analysis. To overcome such

troubles, the hyperbolic tangent function

$$\tanh(s) := \frac{\mathrm{e}^{s} - \mathrm{e}^{-s}}{\mathrm{e}^{s} + \mathrm{e}^{-s}} \tag{1}$$

is utilized as the saturation function in this paper. As the saturation function, the hyperbolic tangent function is continuously differentiable. Some properties of the hyperbolic function are listed in Appendix.

The main theoretical results of this paper are based on the following proposition[18].

Proposition 1. The non-trivial solution of system

$$\begin{cases} \dot{\gamma}_1 &= \gamma_2 \\ \dot{\gamma}_2 &= -\alpha \tanh(k\gamma_1 + l\gamma_2) - \beta \tanh(l\gamma_2) \end{cases} \tag{2}$$

is globally asymptotically stable for any positive numbers α, β, k and l.

In this paper, Proposition 1 is extended into a vector form. Before the extension, it is necessary to define the vector hyperbolic function.

Definition 1. The hyperbolic tangent function for vector $\boldsymbol{x} = [x_1, \cdots, x_n]^{\mathrm{T}}$ is given by

$$\tanh(\boldsymbol{x}) := [\tanh(x_1), \cdots, \tanh(x_n)]^{\mathrm{T}}$$

Proposition 1 can be extended into a vector form as below.

Proposition 2. Consider the vector form of system (2):

$$\begin{cases} \dot{\boldsymbol{\xi}}_1 &= \boldsymbol{\xi}_2 \\ \dot{\boldsymbol{\xi}}_2 &= -\alpha \tanh(k\boldsymbol{\xi}_1 + l\boldsymbol{\xi}_2) - \beta \tanh(l\boldsymbol{\xi}_2) \end{cases} \tag{3}$$

where $\boldsymbol{\xi}_1 \in \mathbf{R}^n$ and $\boldsymbol{\xi}_2 \in \mathbf{R}^n$. The non-trivial solution of system (3) is globally asymptotically stable and semi-globally exponentially stable for any positive numbers α, β, k and l.

Proof of Proposition 2 is presented in Appendix.

Suppose that system (3) is perturbed by a bounded disturbance $\boldsymbol{\Delta}$ with $\|\boldsymbol{\Delta}\| < \bar{\Delta}$:

$$\begin{cases} \dot{\boldsymbol{\xi}}_1 = \boldsymbol{\xi}_2 \\ \dot{\boldsymbol{\xi}}_2 = -\alpha \tanh(k\boldsymbol{\xi}_1 + l\boldsymbol{\xi}_2) - \beta \tanh(l\boldsymbol{\xi}_2) + \boldsymbol{\Delta} \end{cases} \tag{4}$$

The stability property of system (4) can be given in the following proposition.

Proposition 3. Consider the perturbed system (4) with $\boldsymbol{\xi}_1 \in \mathbf{R}^n$ and $\boldsymbol{\xi}_2 \in \mathbf{R}^n$. Let the expected region of attraction be

$$\left\{ [\boldsymbol{\xi}_1^{\mathrm{T}}, \boldsymbol{\xi}_2^{\mathrm{T}}]^{\mathrm{T}} \,\middle|\, \left\| [k\boldsymbol{\xi}_1^{\mathrm{T}} + l\boldsymbol{\xi}_2^{\mathrm{T}}, l\boldsymbol{\xi}_2^{\mathrm{T}}] \right\| < \bar{\mu}, \bar{\mu} > 0 \right\}$$

Then, there exists $\bar{\Delta} > 0$, such that for $\|\boldsymbol{\Delta}\| < \bar{\Delta}$ and positive numbers α, β, k and l, the non-trivial solution of (4) is ultimately bounded.

Proof of Proposition 3 is presented in Appendix.

Remark 1. Under the corresponding definitions in some previous literature[24], the result in Proposition 3 is named local input-to-state stability (LISS) with respect to the perturbation $\boldsymbol{\Delta}$.

2 Problem statement

2.1 Mathematical modeling for a model-scaled helicopter

In this paper, the mathematical model of a model-scaled helicopter presented in our previous research[25] is employed. A simple structure of the model-scaled helicopter is illustrated by Fig. 1 where the two reference frames are defined for mathematical modeling.

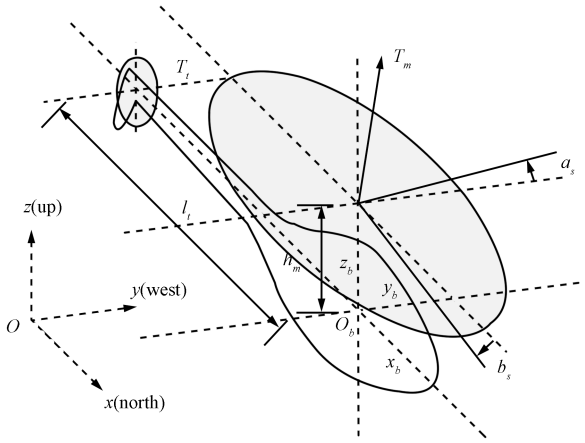

Fig. 1 A simple illustration of the model-scaled helicopter: reference frames, rotor thrusts and flapping angles

The earth reference frame (ERF) is fixed to the earth, with the origin locating at a fix point on the ground. The x axis points to the north and the z axis points upright. The y axis can be confirmed by the right-hand rule.

The fuselage reference frame (FRF) is fixed to the helicopter fuselage. The origin locates at the c.g. (center of gravity) of the helicopter′s fuselage, with the x_b axis pointing to the head of the helicopter. The z_b axis is perpendicular to the x_b axis and points upright. The y_b axis can be confirmed by the right-hand rule.

The mathematical model of the model-scaled helicopter could be derived from the Newton-Euler equations[2, 4]:

$$\dot{\boldsymbol{p}} = \boldsymbol{v} \tag{5}$$

$$m\dot{\boldsymbol{v}} = -m\boldsymbol{g}_3 + R(\boldsymbol{\gamma})\boldsymbol{f} \tag{6}$$

$$\dot{R}(\boldsymbol{\gamma}) = R(\boldsymbol{\gamma})S(\boldsymbol{\omega}) \tag{7}$$

$$J\dot{\boldsymbol{\omega}} = -S(\boldsymbol{\omega})J\boldsymbol{\omega} + \boldsymbol{\tau} \tag{8}$$

where $\boldsymbol{p} := [x, y, z]^{\mathrm{T}}$ and $\boldsymbol{v} := [u, v, w]^{\mathrm{T}}$ are position and velocity of the c.g. of the helicopter in ERF, respectively; m denotes the gross mass; $\boldsymbol{g}_3 := [0, 0, g]^{\mathrm{T}}$, and g is the gravitational acceleration; $\boldsymbol{\gamma} := [\phi, \theta, \psi]^{\mathrm{T}}$ denotes the attitude of the fuselage; the rotational matrix is given by

$$R = [R_{ij}] := \begin{bmatrix} \mathrm{c}\theta\mathrm{c}\psi & \mathrm{c}\psi\mathrm{s}\theta\mathrm{s}\phi - \mathrm{c}\phi\mathrm{s}\psi & \mathrm{c}\phi\mathrm{c}\psi\mathrm{s}\theta + \mathrm{s}\phi\mathrm{s}\psi \\ \mathrm{c}\theta\mathrm{s}\psi & \mathrm{s}\psi\mathrm{s}\theta\mathrm{s}\phi + \mathrm{c}\phi\mathrm{c}\psi & \mathrm{c}\phi\mathrm{s}\psi\mathrm{s}\theta - \mathrm{s}\phi\mathrm{c}\psi \\ -\mathrm{s}\theta & \mathrm{c}\theta\mathrm{s}\phi & \mathrm{c}\theta\mathrm{c}\phi \end{bmatrix}$$

where $\mathrm{c}(\cdot)$ and $\mathrm{s}(\cdot)$ stand for $\cos(\cdot)$ and $\sin(\cdot)$, respectively; $\boldsymbol{\omega} := [p, q, r]^{\mathrm{T}}$ represents the angular velocity in FRF; $S(\cdot)$ denotes the skew-symmetric matrix such that $S(\boldsymbol{\omega})J\boldsymbol{\omega} = \boldsymbol{\omega} \times J\boldsymbol{\omega}$; the inertial matrix is given by

$$J := \begin{bmatrix} I_{xx} & 0 & -I_{xz} \\ 0 & I_{yy} & 0 \\ -I_{xz} & 0 & I_{zz} \end{bmatrix}$$

The resultant force $\boldsymbol{f}$ and torque $\boldsymbol{\tau}$ exerted on the fuselage in FRF are given by

$$\boldsymbol{f} := \begin{bmatrix} T_m\mathrm{s}a_s \\ -T_m\mathrm{s}b_s + T_t \\ T_m\mathrm{c}b_s\mathrm{c}a_s \end{bmatrix} \tag{9}$$

$$\boldsymbol{\tau} := \begin{bmatrix} T_m h_m \mathrm{s}b_s + T_t h_t + Q_m \mathrm{s}a_s \\ T_m l_m + T_m h_m \mathrm{s}a_s + Q_t - Q_m \mathrm{s}b_s \\ -T_m l_m \mathrm{s}b_s - T_t l_t + Q_m \mathrm{c}a_s \mathrm{c}b_s \end{bmatrix} \tag{10}$$

where T_m, Q_m, T_t and Q_t represent thrusts and counteractive torques generated by the main rotor and the tail rotor, respectively; h_m, h_t, l_m and l_t are the vertical and horizonal distances between the c.g. of the helicopter and centers of the rotors, respectively; a_s and b_s are the longitudinal and lateral flapping angles, respectively. The flapping dynamics is negligible in this research since it is extremely fast when compared with the fuselage dynamics. The expressions of rotor thrusts with respect to collective pitches[26] are given by

$$T_i = t_{ci}\rho s_i A_i \Omega_i^2 R_i^2 \tag{11}$$

$$t_{ci} = \frac{1}{4}\left[-\frac{a_i}{4}\sqrt{\frac{s_i}{2}} + \sqrt{\frac{a_i^2 s_i}{32} + \frac{2}{3}a_i\theta_i}\right]^2 \tag{12}$$

and the expressions for torques are given by

$$Q_i = q_{ci}\rho s_i A_i \Omega_i^2 R_i^3 \tag{13}$$

$$q_{ci} = \frac{\delta_d}{8} + 1.13 t_{ci}^{\frac{3}{2}}\sqrt{\frac{s_i}{2}} \tag{14}$$

where subscripts $i = m$ and t represent the main rotor and the tail rotor accordingly; θ_i is collective pitch of the main or tail rotor; ρ, s_i, a_i, Ω_i, A_i and R_i denote the density of the local air, solidity of the rotor disc, slope of the lift curve, rotational rate of rotors, area and radius of the rotor disc, respectively; δ_d is the drag coefficient of the rotor which often has a typical value of 0.012[26].

The mathematical model implies that the motion of the helicopter is controlled by actual controls θ_m, θ_t, a_s and b_s.

2.2 Control objective

In this research, the reference trajectory $\boldsymbol{p}_r = [x_r, y_r, z_r]^{\mathrm{T}}$ to be tracked is smooth, and its derivatives $\boldsymbol{p}_r^{(i)}$ $(i = 1, 2, 3, 4)$ are bounded. The objective is to design a trajectory tracking controller such that

1) The closed-loop system can track the smooth reference trajectory $\boldsymbol{p}_r$ within bounded errors;

2) The main rotor thrust and the attitude satisfy

$$U_t < T_m < U_T \tag{15}$$

$$|\phi| < U_\phi,\ |\theta| < U_\theta \tag{16}$$

where $U_t < mg < U_T \mathrm{c}U_\phi \mathrm{c}U_\theta$.

3 Controller design

The strategy of the controller design can be explained as follows: 1) the helicopter model is simplified into three subsystems, including the altitude subsystem, longitudinal-lateral subsystem and attitude subsystem; 2) a saturated thrust T_m is designed to stabilize the altitude tracking error; 3) a saturated virtual control for the longitudinal-lateral subsystem is designed based on the saturated control thrust; 4) the torque $\boldsymbol{\tau}$ is designed such that the attitude of the fuselage tracks the virtual control for the longitudinal-lateral subsystem. The derivatives of the virtual control are given in explicit forms, and actual controls θ_m, θ_t, a_s and b_s are calculated in the last part of this section.

3.1 Model simplification and transformation

Some simplifications of the helicopter model are required to facilitate the controller design. Since the cyclic flapping angles and the tail rotor thrust are fairly small according to the physical properties of the helicopter[2, 22, 23], it is reasonable to take

$$\boldsymbol{f} \approx [0,\ 0,\ T_m]^{\mathrm{T}} \tag{17}$$

in (9) for simplifying the model, and it follows that

$$m\dot{\boldsymbol{v}} = -m\boldsymbol{g}_3 + \boldsymbol{R}_3(\boldsymbol{\gamma})T_m \tag{18}$$

where $\boldsymbol{R}_3$ denotes the third column of $R(\boldsymbol{\gamma})$, and $\|\boldsymbol{R}_3\| = 1$. Replacing (6) with (18) enables the helicopter model to appear cascaded.

The counteractive torque of the tail rotor Q_t contributes a tiny part of $\boldsymbol{\tau}$, and is also negligible; consequently, torque $\boldsymbol{\tau}$ in (10) can be simplified by

$$\boldsymbol{\tau} = Q_A\boldsymbol{\tau}_A + \boldsymbol{\tau}_B \tag{19}$$

where $\boldsymbol{\tau}_A := [T_t,\ a_s,\ b_s]^{\mathrm{T}}$,

$$Q_A = \begin{bmatrix} h_t & Q_m & T_m h_m \\ 0 & T_m h_m & -Q_m \\ -l_t & 0 & -T_m l_m \end{bmatrix},\ \boldsymbol{\tau}_B = \begin{bmatrix} 0 \\ T_m l_m \\ Q_m \end{bmatrix}$$

Based on (17) and (19), the helicopter model can be devided into three subsystems.

1) The altitude subsystem is obtained by extracting the third equations from (5) and (18):

$$\begin{cases} \dot{z} = w \\ m\dot{w} = -mg + \mathrm{c}\theta\mathrm{c}\phi T_m \end{cases} \tag{20}$$

2) The longitudinal-lateral subsystem is composed of the rest parts of (5) and (18):

$$\begin{cases} \dot{\bar{\boldsymbol{p}}} = \bar{\boldsymbol{v}} \\ m\dot{\bar{\boldsymbol{v}}} = T_m\bar{\boldsymbol{R}}_3 \end{cases} \tag{21}$$

where $\bar{\boldsymbol{p}} := [x, y]^{\mathrm{T}}$, $\bar{\boldsymbol{v}} := [u, v]^{\mathrm{T}}$, and $\bar{\boldsymbol{R}}_3 := [R_{13}, R_{23}]^{\mathrm{T}}$.

3) The attitude subsystem is

$$\dot{\bar{\boldsymbol{R}}}_3 = \hat{R}\bar{\boldsymbol{\omega}} \tag{22}$$

$$\dot{\psi} = \frac{\mathrm{s}\phi}{\mathrm{c}\theta}q + \frac{\mathrm{c}\phi}{\mathrm{c}\theta}r \tag{23}$$

$$J\dot{\boldsymbol{\omega}} = -S(\boldsymbol{\omega})J\boldsymbol{\omega} + \boldsymbol{\tau} \tag{24}$$

where $\bar{\boldsymbol{\omega}} := [p, q]^{\mathrm{T}}$; torque $\boldsymbol{\tau}$ is given by the simplified expression (19), and

$$\hat{R} := \begin{bmatrix} -R_{12} & R_{11} \\ -R_{22} & R_{21} \end{bmatrix} = [\boldsymbol{e}_1, \boldsymbol{e}_2]^{\mathrm{T}} R[-\boldsymbol{e}_2, \boldsymbol{e}_1]$$

$$\boldsymbol{e}_1 := [1, 0, 0]^{\mathrm{T}},\ \boldsymbol{e}_2 := [0, 1, 0]^{\mathrm{T}}$$

The invertibility of $\hat{R}$ can be proved straightforwardly by calculating that $\det(\hat{R}) = -R_{12}R_{21} + R_{11}R_{22} \neq 0$.

Enlightened by [4], we use (22) and (23) to represent the attitude kinematics, where (22) is given by extracting the first two rows from (7), and (23) is the yaw kinematics.

With $\boldsymbol{\gamma}_R := [\bar{\boldsymbol{R}}_3^{\mathrm{T}}, \psi]^{\mathrm{T}}$, the Jacobian matrix satisfies $\|\partial\boldsymbol{\gamma}_R/\partial\boldsymbol{\gamma}\| = \mathrm{c}\theta > 0$ in the case of $|\theta| < \pi/2$. Consequently, the mapping from $\boldsymbol{\gamma}$ to $\boldsymbol{\gamma}_R$ is a local topological homeomorphism, indicating (22) and (23) are capable of representing the attitude kinematics under $|\theta| < \pi/2$. It will be shown that under the proposed control, θ can be maintained in this range.

3.2 Saturated control for altitude subsystem

Define $z_e := z - z_r$ and $w_e := w - \dot{z}_r$. Based on (20), the error dynamics of the altitude subsystem can be given by

$$\begin{cases} \dot{z}_e = w_e \\ \dot{w}_e = -g + \frac{c\theta c\phi}{m} T_m - \ddot{z}_r \end{cases} \tag{25}$$

Proposition 4. Consider the altitude error subsystem (25) with the reference altitude z_r satisfying

$$\frac{U_t}{m} - g + k_z + k_w < |\ddot{z}_r| < \frac{U_T}{m} - g - k_z - k_w \tag{26}$$

Let the expected region of attraction be given by

$$\left\{ [z_e, w_e]^{\mathrm{T}} \, | \|[a_z z_e + a_w w_e, a_w w_e]\| < \bar{z}, \ \bar{z} > 0 \right\}$$

If the positive control parameters k_z, a_z, k_w and a_w are designed such that

$$\min\left[k_z + k_w, \frac{\bar{z}\chi_z}{k_z a_w}, \frac{\bar{z}\chi_z}{k_w a_w + \frac{a_z}{a_w}} \right] > \left| \frac{\mathrm{c}U_\phi \mathrm{c}U_\theta - 1}{m} U_T \right|$$

where $\chi_z = \min\left[\frac{k_z^2 a_w \tanh(\bar{z})^2}{\bar{z}^2}, \frac{k_w a_z \tanh(\bar{z})^2}{a_w \bar{z}^2} \right]$, then the thrust

$$T_m = m\left(g + \ddot{z}_r - k_z \tanh(a_z z_e + a_w w_e) - k_w \tanh(a_w w_e)\right) \tag{27}$$

assures the following statements:

1) The altitude tracking error z_e is ultimately bounded, if $|\phi| < U_\phi$ and $|\theta| < U_\theta$;

2) The constraint given by (15) is satisfied.

Proof.

1) Substituting (27) into (25) yields

$$\begin{cases} \dot{z}_e = w_e \\ \dot{w}_e = -k_z \tanh(a_z z_e + a_w w_e) - k_w \tanh(a_w w_e) + \delta_z \end{cases} \tag{28}$$

where $|\delta_z| < \frac{1 - \mathrm{c}U_\phi \mathrm{c}U_\theta}{m} U_T$. Following the steps of Proposition 3 can complete the proof.

2) Satisfaction of constraint (15) can be proved by substituting (26) into (27). □

Remark 2. The implication of (26) is intuitive. If the control force is subject to constraints, the acceleration is obviously limited.

Remark 3. If $\phi = \theta = 0$, substituting (27) into (25) yields

$$\begin{cases} \dot{z}_e = w_e \\ \dot{w}_e = -k_z \tanh(a_z z_e + a_w w_e) - k_w \tanh(a_w w_e) \end{cases} \tag{29}$$

which satisfies the requirements of Proposition 2, and can be proved to be globally asymptotically stable and semi-globally exponentially stable.

3.3 Saturated control for longitudinal-lateral subsystem

Define $\bar{\boldsymbol{p}}_r := [x_r, y_r]^{\mathrm{T}}$, $\bar{\boldsymbol{p}}_e := \bar{\boldsymbol{p}} - \bar{\boldsymbol{p}}_r$, $\bar{\boldsymbol{v}}_e := \bar{\boldsymbol{v}} - \dot{\bar{\boldsymbol{p}}}_r$, and $\bar{\boldsymbol{R}}_{3e} := \bar{\boldsymbol{R}}_3 - \bar{\boldsymbol{\alpha}}_P$, where $\bar{\boldsymbol{\alpha}}_P$ is the virtual control. Based on (21), the error dynamics of the longitudinal-lateral subsystem can be given by

$$\begin{cases} \dot{\bar{\boldsymbol{p}}}_e = \bar{\boldsymbol{v}}_e \\ \dot{\bar{\boldsymbol{v}}}_e = \frac{T_m}{m} \bar{\boldsymbol{\alpha}}_P + \frac{T_m}{m} \bar{\boldsymbol{R}}_{3e} - \ddot{\bar{\boldsymbol{p}}}_r \end{cases} \tag{30}$$

Proposition 5. Consider the longitudinal-lateral error subsystem (30) with the reference longitudinal-lateral trajectory satisfying

$$\|\ddot{\bar{\boldsymbol{p}}}_r\| < \frac{U_t M_R}{m} - \sqrt{2} k_p - \sqrt{2} k_v \tag{31}$$

where $k_p > 0$, $k_v > 0$, and $M_R > 0$. Let the expected region of attraction be given by

$$\left\{ [\bar{\boldsymbol{p}}_e^{\mathrm{T}}, \bar{\boldsymbol{v}}_e^{\mathrm{T}}]^{\mathrm{T}} \, \middle| \, \left\| [a_p \bar{\boldsymbol{p}}_e^{\mathrm{T}} + a_v \bar{\boldsymbol{v}}_e^{\mathrm{T}}, a_v \bar{\boldsymbol{v}}_e^{\mathrm{T}}] \right\| < \bar{p}, \ \bar{p} > 0 \right\}$$

where $a_v > 0$ and $a_p > 0$. Denote

$$\delta_R := \min\left[\frac{m(k_p + k_v)}{U_T}, \frac{m\bar{p}\chi_p}{k_p a_v U_T}, \frac{m\bar{p}\chi_p}{(k_v a_v + \frac{a_p}{a_v}) U_T} \right] \tag{32}$$

where $\chi_p = \min\left[\frac{k_p^2 a_v \tanh(\bar{p})^2}{\bar{p}^2}, \frac{k_v a_p \tanh(\bar{p})^2}{a_v \bar{p}^2} \right]$, and set the control parameters such that $\arcsin(M_R + \delta_R) < U_\phi$ and $\arcsin(M_R + \delta_R) < U_\theta$. If the attitude tracking error satisfies $\|\bar{\boldsymbol{R}}_{3e}\| < \delta_R$, then the virtual control

$$\bar{\boldsymbol{\alpha}}_P = \frac{m}{T_m} \left(\ddot{\bar{\boldsymbol{p}}}_r - k_p \tanh(a_p \bar{\boldsymbol{p}}_e + a_v \bar{\boldsymbol{v}}_e) - k_v \tanh(a_v \bar{\boldsymbol{v}}_e) \right) \tag{33}$$

guarantees the following statements:

1) The tracking error $\bar{\boldsymbol{p}}_e$ is ultimately bounded;

2) The constraints given by (16) are satisfied.

Proof.

1) Substitution of (33) into (30) yields

$$\begin{cases} \dot{\bar{\boldsymbol{p}}}_e = \bar{\boldsymbol{v}}_e \\ \dot{\bar{\boldsymbol{v}}}_e = -k_p \tanh(a_p \bar{\boldsymbol{p}}_e + a_v \bar{\boldsymbol{v}}_e) - k_v \tanh(a_v \bar{\boldsymbol{v}}_e) + \\ \qquad \frac{T_m}{m} \bar{\boldsymbol{R}}_{3e} \end{cases}$$

where the boundedness of $\bar{\boldsymbol{R}}_{3e}$ is assumed by (32), and the boundedness of T_m is proved in Proposition 4. The ultimate boundedness of $\bar{\boldsymbol{p}}_e$ can be proved by using the results of Proposition 3.

2) Substituting (31) into (33) yields

$$\|\bar{\boldsymbol{\alpha}}_P\| < \frac{m}{U_t} \left(\|\ddot{\bar{\boldsymbol{p}}}_r\| + \sqrt{2} k_p + \sqrt{2} k_v \right) < M_R$$

implying that

$$\begin{aligned} (M_R + \delta_R)^2 > & \|\bar{\boldsymbol{R}}_3\|^2 = R_{31}^2 + R_{32}^2 = \\ & (\mathrm{c}\phi \mathrm{c}\psi \mathrm{s}\theta + \mathrm{s}\phi \mathrm{s}\psi)^2 + (\mathrm{c}\phi \mathrm{s}\psi \mathrm{s}\theta - \mathrm{s}\phi \mathrm{c}\psi)^2 = \\ & \mathrm{c}^2\phi \mathrm{s}^2\theta + \mathrm{s}^2\phi \end{aligned}$$

On the one hand,

$$(M_R + \delta_R)^2 > \mathrm{c}^2\phi \mathrm{s}^2\theta + \mathrm{s}^2\phi \geq \mathrm{s}^2\phi$$

indicating $|\phi| \leq \arcsin(M_R + \delta_R)$, on the other hand

$$(M_R + \delta_R)^2 > \mathrm{c}^2\phi \mathrm{s}^2\theta + \mathrm{s}^2\phi \geq \mathrm{c}^2\phi \mathrm{s}^2\theta + \mathrm{s}^2\phi \mathrm{s}^2\theta = \mathrm{s}^2\theta$$

implying that $|\theta| \leq \arcsin(M_R + \delta_R)$. Consequently, by setting $\arcsin(M_R + \delta_R) < U_\phi$ and $\arcsin(M_R + \delta_R) < U_\theta$, the constraint for attitude is satisfied. □

Remark 4. When $\bar{\boldsymbol{R}}_{3e} = 0$, substituting (33) into (30) yields

$$\begin{cases} \dot{\bar{\boldsymbol{p}}}_e = \bar{\boldsymbol{v}}_e \\ \dot{\bar{\boldsymbol{v}}}_e = -k_p \tanh(a_p \bar{\boldsymbol{p}}_e + a_v \bar{\boldsymbol{v}}_e) - k_v \tanh(a_v \bar{\boldsymbol{v}}_e) \end{cases} \tag{34}$$

It satisfies conditions of Proposition 2, indicating that $\bar{\boldsymbol{p}}_e$ is globally asymptotically stable and semi-globally exponentially stable.

3.4 Backstepping design for attitude subsystem

In the preceding subsections, we have obtained the main rotor thrust T_m and the virtual control $\bar{\boldsymbol{\alpha}}_P$. The main rotor thrust T_m can be implemented, while $\bar{\boldsymbol{\alpha}}_P$ is the reference signal to be tracked by the attitude subsystem.

Select the Lyapunov candidate

$$L_2 = \frac{1}{2}\bar{\boldsymbol{R}}_{3e}^{\mathrm{T}}\bar{\boldsymbol{R}}_{3e} + \frac{k_{\gamma i}}{2}\int_0^t \bar{\boldsymbol{R}}_{3e}^{\mathrm{T}}\mathrm{d}t \int_0^t \bar{\boldsymbol{R}}_{3e}\mathrm{d}t$$

where $k_{\gamma i} > 0$ are the parameters to be designed. Its derivative

$$\begin{aligned}\dot{L}_2 = \ & \bar{\boldsymbol{R}}_{3e}^{\mathrm{T}}\dot{\bar{\boldsymbol{R}}}_{3e} + k_{\gamma i}\bar{\boldsymbol{R}}_{3e}^{\mathrm{T}}\int_0^t \bar{\boldsymbol{R}}_{3e}\mathrm{d}t = \\ & \bar{\boldsymbol{R}}_{3e}^{\mathrm{T}}(\dot{\bar{\boldsymbol{R}}}_3 - \dot{\bar{\boldsymbol{\alpha}}}_P) + k_{\gamma i}\bar{\boldsymbol{R}}_{3e}^{\mathrm{T}}\int_0^t \bar{\boldsymbol{R}}_{3e}\mathrm{d}t = \\ & \bar{\boldsymbol{R}}_{3e}^{\mathrm{T}}(\hat{R}\bar{\boldsymbol{\omega}} - \dot{\bar{\boldsymbol{\alpha}}}_P) + k_{\gamma i}\bar{\boldsymbol{R}}_{3e}^{\mathrm{T}}\int_0^t \bar{\boldsymbol{R}}_{3e}\mathrm{d}t\end{aligned}$$

Define $\bar{\boldsymbol{\omega}}_e := \bar{\boldsymbol{\omega}} - \bar{\boldsymbol{\alpha}}_R$, where $\bar{\boldsymbol{\alpha}}_R$ denotes the virtual control for attitude kinematics. With the virtual control for attitude kinematics designed by

$$\bar{\boldsymbol{\alpha}}_R = \hat{R}^{-1}\left(-k_{\gamma p}\bar{\boldsymbol{R}}_{3e} - k_{\gamma i}\int_0^t \bar{\boldsymbol{R}}_{3e}\mathrm{d}t + \dot{\bar{\boldsymbol{\alpha}}}_P\right) \tag{35}$$

where $k_{\gamma p} > 0$ and $k_{\gamma i} > 0$ are control parameters, the derivative of L_2 is then calculated by

$$\begin{aligned}\dot{L}_2 = & \bar{\boldsymbol{R}}_{3e}^{\mathrm{T}}(\hat{R}\boldsymbol{\alpha}_R + \hat{R}\bar{\boldsymbol{\omega}}_e - \dot{\bar{\boldsymbol{\alpha}}}_R) + k_{\gamma i}\bar{\boldsymbol{R}}_{3e}^{\mathrm{T}}\int_0^t \bar{\boldsymbol{R}}_{3e}\mathrm{d}t = \\ & - k_{\gamma p}\bar{\boldsymbol{R}}_{3e}^{\mathrm{T}}\bar{\boldsymbol{R}}_{3e} + \bar{\boldsymbol{R}}_{3e}^{\mathrm{T}}\hat{R}\bar{\boldsymbol{\omega}}_e\end{aligned}$$

Before the backstepping design for the attitude dynamics, the controller for the yaw angle ψ should be designed. The reference yaw angle ψ_r is designed by

$$\psi_r = \mathrm{atan2}(\dot{y}_r, \dot{x}_r) \tag{36}$$

such that the helicopter head always points to the tangent of the reference trajectory.

Consider the yaw angle kinematics given by (23), where r is regarded as the virtual control. Define $\psi_e := \psi - \psi_r$ and choose the Lyapunov candidate

$$L_3 = L_2 + \frac{1}{2}\psi_e^2 + \frac{k_{\psi i}}{2}\left(\int_0^t \psi_e\mathrm{d}t\right)^2$$

It follows that

$$\begin{aligned}\dot{L}_3 = & \dot{L}_2 + \psi_e\dot{\psi}_e + k_{\psi i}\psi_e\int_0^t \psi_e\mathrm{d}t = \\ & \dot{L}_2 + \psi_e(\dot{\psi} - \dot{\psi}_r) + k_{\psi i}\psi_e\int_0^t \psi_e\mathrm{d}t = \\ & \dot{L}_2 + \psi_e(\frac{\mathrm{s}\phi}{\mathrm{c}\theta}q + \frac{\mathrm{c}\phi}{\mathrm{c}\theta}r - \dot{\psi}_r) + k_{\psi i}\psi_e\int_0^t \psi_e\mathrm{d}t\end{aligned}$$

If the virtual control $\alpha_\psi = r - r_e$ is designed by

$$\alpha_\psi = \frac{-\mathrm{s}\phi}{\mathrm{c}\phi}q - \frac{\mathrm{c}\theta}{\mathrm{c}\phi}\left(k_{\psi p}\psi_e + k_{\psi i}\int_0^t \psi_e\mathrm{d}t - \dot{\psi}_r\right) \tag{37}$$

where $k_{\psi p} > 0$ and $k_{\psi i} > 0$ are control parameters, then

$$\dot{L}_3 = -k_{\gamma p}\bar{\boldsymbol{R}}_{3e}^{\mathrm{T}}\bar{\boldsymbol{R}}_{3e} - k_{\psi p}\psi_e^2 + \bar{\boldsymbol{R}}_{3e}^{\mathrm{T}}\hat{R}\bar{\boldsymbol{\omega}}_e + \frac{\mathrm{c}\phi}{\mathrm{c}\theta}\psi_e r_e$$

Define the reference signals to be tracked by the attitude dynamics as

$$\boldsymbol{\alpha}_R := [\bar{\boldsymbol{\alpha}}_R^{\mathrm{T}},\ \alpha_\psi]^{\mathrm{T}} \tag{38}$$

Define also the tracking error of attitude dynamics as

$$\boldsymbol{\omega}_e := [\bar{\boldsymbol{\omega}}_e^{\mathrm{T}},\ r_e]^{\mathrm{T}} = \boldsymbol{\omega} - \boldsymbol{\alpha}_R \tag{39}$$

Select the Lyapunov candidate

$$L_4 = L_3 + \frac{1}{2}\boldsymbol{\omega}_e^{\mathrm{T}}J\boldsymbol{\omega}_e + \frac{k_{\omega i}}{2}\int_0^t \boldsymbol{\omega}_e^{\mathrm{T}}\mathrm{d}t\int_0^t \boldsymbol{\omega}_e\mathrm{d}t$$

Its derivative is

$$\begin{aligned}\dot{L}_4 = & \dot{L}_3 + \boldsymbol{\omega}_e^{\mathrm{T}}J\dot{\boldsymbol{\omega}}_e + k_{\omega i}\boldsymbol{\omega}_e^{\mathrm{T}}\int_0^t \boldsymbol{\omega}_e\mathrm{d}t = \\ & \dot{L}_3 + \boldsymbol{\omega}_e^{\mathrm{T}}(-S(\boldsymbol{\omega})J\boldsymbol{\omega} + \boldsymbol{\tau} - J\dot{\boldsymbol{\alpha}}_R) + k_{\omega i}\boldsymbol{\omega}_e^{\mathrm{T}}\int_0^t \boldsymbol{\omega}_e\mathrm{d}t\end{aligned}$$

Design the torque as

$$\boldsymbol{\tau} = S(\boldsymbol{\omega})J\boldsymbol{\omega} + J\dot{\boldsymbol{\alpha}}_R - k_{\omega p}\boldsymbol{\omega}_e - k_{\omega i}\int_0^t \boldsymbol{\omega}_e\mathrm{d}t - G_\gamma\bar{\boldsymbol{\gamma}}_e \tag{40}$$

where

$$G_\gamma = \begin{bmatrix} \hat{R} & 0_{2\times 1} \\ 0_{1\times 2} & \frac{\mathrm{c}\phi}{\mathrm{c}\theta} \end{bmatrix}$$

and $\bar{\boldsymbol{\gamma}}_e := [\bar{\boldsymbol{R}}_{3e}^{\mathrm{T}},\ \psi_e]^{\mathrm{T}}$. $k_{\omega p} > 0$ and $k_{\omega p} > 0$ are the control parameters. Then,

$$\dot{L}_4 = -k_{\gamma p}\bar{\boldsymbol{R}}_{3e}^{\mathrm{T}}\bar{\boldsymbol{R}}_{3e} - k_{\psi p}\psi_e^2 - k_{\omega p}\boldsymbol{\omega}_e^{\mathrm{T}}\boldsymbol{\omega}_e \le 0 \tag{41}$$

implying that the backstepping process is completed.

Proposition 6. Consider the attitude subsystem given by (22), (23) and (24). Under the controller designed by (35), (37), (38) and (40), the attitude of the helicopter fuselage can track $\bar{\boldsymbol{\alpha}}_P$ and ψ_r exponentially.

Proof. Take L_4 as the Lyapunov function for the attitude subsystem. The derivative of L_4 can be given by (41), implying that $\bar{\boldsymbol{R}}_{3e} \in \mathcal{L}_2 \cap \mathcal{L}_\infty$ and $\psi_e \in \mathcal{L}_2 \cap \mathcal{L}_\infty$. Since all signals are uniformly continuous, $\bar{\boldsymbol{R}}_{3e}$ and ψ_e are asymptotically stable according to the Barbalat lemma. Further, $\bar{\boldsymbol{R}}_{3e}$ and ψ_e are exponentially stable because L_4 and $\dot{L}_4$ are in quadratic forms. □

3.5 Derivatives of virtual control

Prohibitive expressions for derivatives of the virtual control often impede applications of backstepping control to high order systems. In this research, however, the explicit expressions can be obtained for derivatives of the virtual controls $\dot{\bar{\alpha}}_P$ and $\dot{\alpha}_R$ without in (35) and (40), avoiding the use of numerical differentiators.

The derivatives for T_m are calculated by

$$\begin{aligned}\dot{T}_m = & m\left[z_r^{(3)} - k_w\frac{\mathrm{d}\tanh(a_w w_e)}{\mathrm{d}(a_w w_e)}(a_w\dot{w}_e) - \right. \\ & \left. k_z\frac{\mathrm{d}\tanh(a_z z_e + a_w w_e)}{\mathrm{d}(a_z z_e + a_w w_e)}(a_z\dot{z}_e + a_w\dot{w}_e)\right]\end{aligned} \tag{42}$$

$$\begin{aligned}\ddot{T}_m = & m\left[z_r^{(4)} - k_z\frac{\mathrm{d}^2\tanh(a_z z_e + a_w w_e)}{\mathrm{d}(a_z z_e + a_w w_e)^2}(a_z\dot{z}_e + a_w\dot{w}_e)^2 - \right. \\ & k_z\frac{\mathrm{d}\tanh(a_z z_e + a_w w_e)}{\mathrm{d}(a_z z_e + a_w w_e)}(a_z\ddot{z}_e + a_w\ddot{w}_e) - \\ & \left. k_w\ \frac{\mathrm{d}^2\tanh(a_w w_e)}{\mathrm{d}(a_w w_e)^2}(a_w\dot{w}_e)^2 - k_w\frac{\mathrm{d}\tanh(a_w w_e)}{\mathrm{d}(a_w w_e)}(a_w\ddot{w}_e)\right]\end{aligned} \tag{43}$$

where $\ddot{z}_e = \dot{w}_e = \frac{\dot{T}_m}{m} - g - \ddot{z}_r$, and $\ddot{w}_e = \frac{\ddot{T}_m}{m} - z_r^{(3)}$.

Taking $\boldsymbol{r}_1 = \ddot{\bar{\boldsymbol{p}}}_r - k_p \tanh(a_p \bar{\boldsymbol{p}}_e + a_v \bar{\boldsymbol{v}}_e) - k_v \tanh(a_v \bar{\boldsymbol{v}}_e)$ and $\bar{r}_1 = 1/T_m$ yields that $\bar{\boldsymbol{\alpha}}_P = m\bar{r}_1 \boldsymbol{r}_1$. It follows that

$$\dot{\bar{\boldsymbol{\alpha}}}_P = m\left(\dot{\bar{r}}_1 \boldsymbol{r}_1 + \bar{r}_1 \dot{\boldsymbol{r}}_1\right) \tag{44}$$

$$\ddot{\bar{\boldsymbol{\alpha}}}_P = m\left(\ddot{\bar{r}}_1 \boldsymbol{r}_1 + 2\dot{\bar{r}}_1 \dot{\boldsymbol{r}}_1 + \bar{r}_1 \ddot{\boldsymbol{r}}_1\right) \tag{45}$$

The derivatives for $\bar{r}_1$ are given by

$$\dot{\bar{r}}_1 = -\frac{1}{T_m^2}\dot{T}_m,\ \ddot{\bar{r}}_1 = -\frac{1}{T_m^2}\ddot{T}_m + \frac{2}{T_m^3}\dot{T}_m$$

where $\dot{T}_m$ and $\ddot{T}_m$ are obtained by (42) and (43), respectively. The derivatives of $\boldsymbol{r}_1$ are given by

$$\begin{aligned}\dot{\boldsymbol{r}}_1 =& \bar{\boldsymbol{p}}_r^{(3)} - k_v \frac{\mathrm{dtanh}(a_v \bar{\boldsymbol{v}}_e)}{\mathrm{d}(a_v \bar{\boldsymbol{v}}_e)}(a_v \dot{\bar{\boldsymbol{v}}}_e) - \\ & k_p \frac{\mathrm{dtanh}(a_p \bar{\boldsymbol{p}}_e + a_v \bar{\boldsymbol{v}}_e)}{\mathrm{d}(a_p \bar{\boldsymbol{p}}_e + a_v \bar{\boldsymbol{v}}_e)}(a_p \dot{\bar{\boldsymbol{p}}}_e + a_v \dot{\bar{\boldsymbol{v}}}_e)\end{aligned} \tag{46}$$

$$\begin{aligned}\ddot{\boldsymbol{r}}_1 =& \bar{\boldsymbol{p}}_r^{(4)} - k_v \frac{\mathrm{dtanh}(a_v \bar{\boldsymbol{v}}_e)}{\mathrm{d}(a_v \bar{\boldsymbol{v}}_e)}(a_v \ddot{\bar{\boldsymbol{v}}}_e) - \\ & k_v \frac{\mathrm{d}^2\tanh(a_v \bar{\boldsymbol{v}}_e)}{\mathrm{d}(a_v \bar{\boldsymbol{v}}_e)^2}(a_v \dot{\bar{\boldsymbol{v}}}_e)^2 - \\ & k_p \frac{\mathrm{d}^2\tanh(a_p \bar{\boldsymbol{p}}_e + a_v \bar{\boldsymbol{v}}_e)}{\mathrm{d}(a_p \bar{\boldsymbol{p}}_e + a_v \bar{\boldsymbol{v}}_e)^2}(a_p \dot{\bar{\boldsymbol{p}}}_e + a_v \dot{\bar{\boldsymbol{v}}}_e)^2 - \\ & k_p \frac{\mathrm{dtanh}(a_p \bar{\boldsymbol{p}}_e + a_v \bar{\boldsymbol{v}}_e)}{\mathrm{d}(a_p \bar{\boldsymbol{p}}_e + a_v \bar{\boldsymbol{v}}_e)}(a_p \ddot{\bar{\boldsymbol{p}}}_e + a_v \ddot{\bar{\boldsymbol{v}}}_e)\end{aligned} \tag{47}$$

where $\ddot{\bar{\boldsymbol{p}}}_e = \dot{\bar{\boldsymbol{v}}}_e = -\ddot{\bar{\boldsymbol{p}}}_r + \frac{T_m}{m}\bar{\boldsymbol{R}}_3$, and $\ddot{\bar{\boldsymbol{v}}}_e = -\bar{\boldsymbol{p}}_r^{(3)} + \frac{\dot{T}_m}{m}\bar{\boldsymbol{R}}_3 + \frac{T_m}{m}\dot{\bar{\boldsymbol{R}}}_3$. The derivative of the vector hyperbolic function with respect to vector is defined in Definition A2 in Appendix.

Next, the derivative of the virtual control for $\bar{\boldsymbol{\alpha}}_R$ can be yielded by

$$\begin{aligned}\dot{\bar{\boldsymbol{\alpha}}}_R =& \left[\frac{\mathrm{d}}{\mathrm{d}t}\left(\hat{R}^{-1}\right)\right]\hat{R}\bar{\boldsymbol{\alpha}}_R + \\ & \hat{R}^{-1}\left(-k_{\gamma p}\dot{\bar{\boldsymbol{R}}}_{3e} - k_{\gamma i}\bar{\boldsymbol{R}}_{3e} + \ddot{\bar{\boldsymbol{\alpha}}}_P\right) = \\ & -\hat{R}^{-1}\dot{\hat{R}}\bar{\boldsymbol{\alpha}}_R + \hat{R}^{-1}\left(-k_{\gamma p}\dot{\bar{\boldsymbol{R}}}_{3e} - k_{\gamma i}\bar{\boldsymbol{R}}_{3e} + \ddot{\bar{\boldsymbol{\alpha}}}_P\right)\end{aligned} \tag{48}$$

where

$$\dot{\hat{R}} = [\boldsymbol{e}_1, \boldsymbol{e}_2]^{\mathrm{T}} R S(\boldsymbol{\omega})[-\boldsymbol{e}_2, \boldsymbol{e}_1],\ \dot{\bar{\boldsymbol{R}}}_{3e} = \hat{R}\bar{\boldsymbol{\omega}} - \dot{\bar{\boldsymbol{\alpha}}}_P$$

and $\ddot{\bar{\boldsymbol{\alpha}}}_P$ is obtained by (45). The derivative of the virtual control for yaw angle can be acquired by

$$\begin{aligned}\dot{\alpha}_\psi =& -\frac{\dot{\phi}q}{\mathrm{c}^2\phi} - \frac{\mathrm{s}\phi}{\mathrm{c}\phi}\dot{q} - \frac{\mathrm{c}\theta}{\mathrm{c}\phi}\left(k_{\psi p}\dot{\psi}_e + k_{\psi i}\psi_e - \ddot{\psi}_r\right) + \\ & \frac{\mathrm{s}\theta\mathrm{c}\phi\dot{\theta} + \mathrm{c}\theta\mathrm{s}\phi\dot{\phi}}{\mathrm{c}^2\phi}\left(k_{\psi p}\psi_e + k_{\psi i}\int_0^t \psi_e \mathrm{d}t - \dot{\psi}_r\right)\end{aligned} \tag{49}$$

where

$$\begin{aligned}\dot{\psi}_r =& \frac{\ddot{x}_r\dot{y}_r - \dot{x}_r\ddot{y}_r}{\dot{x}_r^2 + \dot{y}_r^2} \\ \ddot{\psi}_r =& \frac{\left(\dddot{x}_r\dot{y}_r - \dot{x}_r\dddot{y}_r\right)\left(\dot{x}_r^2 + \dot{y}_r^2\right)}{\left(\dot{x}_r^2 + \dot{y}_r^2\right)^2} - \\ & \frac{\left(\ddot{x}_r\dot{y}_r - \dot{x}_r\ddot{y}_r\right)\left(2\dot{x}_r\ddot{x}_r + 2\dot{y}_r\ddot{y}_r\right)}{\left(\dot{x}_r^2 + \dot{y}_r^2\right)^2} \\ \dot{\psi}_e =& \frac{\mathrm{s}\phi}{\mathrm{c}\theta}q + \frac{\mathrm{c}\phi}{\mathrm{c}\theta}r - \dot{\psi}_r\end{aligned}$$

In (49), $\dot{\phi}$ and $\dot{\theta}$ are given by

$$\dot{\boldsymbol{\gamma}} = R_r^{-1}\boldsymbol{\omega}$$

where

$$R_r := \begin{bmatrix} 1 & 0 & -\mathrm{s}\theta \\ 0 & \mathrm{c}\phi & \mathrm{c}\theta\mathrm{s}\phi \\ 0 & -\mathrm{s}\phi & \mathrm{c}\theta\mathrm{c}\phi \end{bmatrix}$$

is the transformation matrix for the attitude from ERF to FRF.

In summary, the derivative of virtual control for $\bar{\boldsymbol{\alpha}}_P$ is obtained by (44), and the derivative of virtual control for α_R is yielded by

$$\dot{\boldsymbol{\alpha}}_R = [\dot{\bar{\boldsymbol{\alpha}}}_R^{\mathrm{T}}, \dot{\alpha}_\psi]^{\mathrm{T}} \tag{50}$$

where derivatives $\dot{\bar{\boldsymbol{\alpha}}}_R$ and $\dot{\alpha}_\psi$ are calculated by (48) and (49), respectively.

Remark 5. Actually, $\dot{\boldsymbol{\alpha}}_P$ and $\ddot{\boldsymbol{\alpha}}_P$ are bounded. In the expressions for derivatives of virtual controls, all the first-order and second-order partial derivatives of hyperbolic tangent functions are bounded, as are given in Property A2 in Appendix. The derivatives of reference trajectory are bounded, as are stated in the control objective. The derivatives of tracking errors are bounded, since the closed-loop expressions are composed of hyperbolic tangent functions.

3.6 Calculating the actual controls

In the previous subsections, the control thrust T_m and torque $\boldsymbol{\tau}$ are obtained by (27) and (40). Consequently, the actual controls θ_m, θ_t, a_s, and b_s can be calculated from the thrust and torque through the following steps.

θ_m can be obtained from (11):

$$t_{cm} = \frac{T_m}{\rho s_m A_m \Omega_m^2 R_m^2},\ \theta_m = \frac{3}{2}\left[\sqrt{\frac{s_m t_{cm}}{2}} + \frac{4t_{cm}}{a_m}\right] \tag{51}$$

and Q_m is determined by

$$q_{cm} = \frac{\delta}{8} + 1.13 t_{cm}^{\frac{3}{2}}\sqrt{\frac{s_m}{2}},\ Q_m = q_{cm}\rho s_m A_m \Omega_m^2 R_m^3$$

Then, $\boldsymbol{\tau}_A = [T_t, a_s, b_s]^{\mathrm{T}}$ can be calculated by using (19)

$$\boldsymbol{\tau}_A = Q_A^{-1}(\boldsymbol{\tau} - \boldsymbol{\tau}_B) \tag{52}$$

In (52), the invertibility of Q_A can be proved by

$$\det Q_A = l_t Q_m^2 + (h_m l_t - h_t l_m) h_m T_m^2 \neq 0$$

where $h_m \gg l_m$ and $l_t \gg h_t$, according to the physical structure of typical helicopters.

And the collective pitch of the tail rotor is yielded by

$$t_{ct} = \frac{T_t}{\rho s_t A_t \Omega_t^2 R_t^2},\ \theta_t = \frac{3}{2}\left[\sqrt{\frac{s_t t_{ct}}{2}} + \frac{4t_{ct}}{a_t}\right] \tag{53}$$

4 Analysis on closed-loop system

In this section, a stability analysis is provided for the closed-loop system with neglected terms. In advance, the main rotor thrust and fuselage attitude are proved to satisfy constraints (15) and (16).

In Subsection 3.1, the forces and torques are simplified such that the helicopter model appears cascaded. The small

neglected terms can be explicitly written by

$$\boldsymbol{\Delta}_f = \begin{bmatrix} T_m \mathrm{s}a_s \\ -T_m \mathrm{s}b_s + T_t \\ T_m(\mathrm{c}a_s \mathrm{c}b_s - 1) \end{bmatrix} \tag{54}$$

$$\boldsymbol{\Delta}_\tau := \begin{bmatrix} Q_m(\mathrm{s}a_s - a_s) + T_m h_m(\mathrm{s}b_s - b_s) \\ Q_t - Q_m(\mathrm{s}b_s - b_s) + T_m h_m(\mathrm{s}a_s - a_s) \\ -Q_m(1 - \mathrm{c}a_s \mathrm{c}b_s) + T_m l_m(b_s - \mathrm{s}b_s) \end{bmatrix} \tag{55}$$

which are functions of actual controls. It is noticeable that if $a_s = 0$ and $b_s = 0$, there are $\|\boldsymbol{\Delta}_f\| = |T_t|$ and $\|\boldsymbol{\Delta}_\tau\| = |Q_t|$. The tail rotor thrust T_t is bounded, because $|T_t| \ll |T_m| < U_T$. The tail rotor torque Q_t can be proved bounded by considering (11)∼(14). Meanwhile, cyclic pitch angles a_s and b_s are responsible for manipulating pitch and roll motion of the fuselage, so that they are functions of $\boldsymbol{\zeta} := [\|\bar{\boldsymbol{R}}_{3e}\|, |\psi_e|, \|\boldsymbol{\omega}_e\|]^{\mathrm{T}}$. As given in some literature[1−2, 22], $\boldsymbol{\Delta}_f$ and $\boldsymbol{\Delta}_\tau$ are very small; consequently, some conservative bounds on $\boldsymbol{\Delta}_f$ and $\boldsymbol{\Delta}_\tau$ can be estimated as

$$\|\boldsymbol{\Delta}_f\| < l_v\|\boldsymbol{\zeta}\| + \bar{\Delta}_f,\ \|\boldsymbol{\Delta}_\tau\| < l_\omega\|\boldsymbol{\zeta}\| + \bar{\Delta}_\tau \tag{56}$$

where l_v, l_ω, $\bar{\Delta}_f$ and $\bar{\Delta}_\tau$ are small positive numbers. In (56), the non-vanishing terms $\bar{\Delta}_f$ and $\bar{\Delta}_\tau$ concern the values of $|T_t|$ and $|Q_t|$, which are very small according to the physical properties of typical helicopters. The vanishing terms $l_v\|\boldsymbol{\zeta}\|$ and $l_\omega\|\boldsymbol{\zeta}\|$ depend on the fact that $\boldsymbol{\Delta}_f$ and $\boldsymbol{\Delta}_\tau$ are related to the attitude tracking errors.

Proposition 7. Consider the helicopter plant (5)∼(8), with forces and torques given by (9) and (10). Suppose that the reference trajectories satisfy (26) and (31). If the controller is designed by (27), (33), (35), (37), (38), (40), (44), (45), (48)∼(50) and (51)∼(53), then

1) The main rotor thrust satisfies constraint (15);

2) The fuselage attitude satisfies constraint (16) after a finite time;

3) Tracking errors z_e and $\bar{\boldsymbol{p}}_e$ are ultimately bounded.

Proof. Substituting (26) into (27) proves 1) directly.

The virtual control expressed by (33) is bounded, because of the bounded T_m and reference signal satisfying (31). Take L_4 as the Lyapunov function for the attitude subsystem. Based on Proposition 6, the derivative of L_4 is given by

$$\begin{aligned} \dot{L}_4 < &- k_{\min}\|\boldsymbol{\zeta}\|^2 + l_\omega\|\boldsymbol{\zeta}\|^2 + \bar{\Delta}_\tau\|\boldsymbol{\zeta}\| = \\ &- (k_{\min} - l_\omega)\|\boldsymbol{\zeta}\|^2 + \bar{\Delta}_\tau\|\boldsymbol{\zeta}\| \end{aligned}$$

where $k_{\min} = \min[k_{\gamma p},\ k_{\psi p},\ k_{\omega p}]$. Since l_ω is very small, it is always possible to find a proper $k_{\min}$ such that $k_{\min} - l_\omega > 0$, and ζ is ultimately bounded by $\|\boldsymbol{\zeta}\| < \frac{\bar{\Delta}_\tau}{k_{\min} - l_\omega}$. The ultimate boundedness of $\boldsymbol{\zeta}$ implies that $\|\bar{\boldsymbol{R}}_{3e}\| < \frac{\bar{\Delta}_\tau}{k_{\min} - l_\omega}$ after a finite time T_1. Set $k_{\gamma p}$, $k_{\psi p}$ and $k_{\omega p}$ such that

$$\begin{aligned} \frac{\bar{\Delta}_\tau}{k_{\min} - l_\omega} + \|\boldsymbol{\Delta}_f\| < \frac{\bar{\Delta}_\tau}{k_{\min} - l_\omega} + l_v\|\boldsymbol{\zeta}\| + \bar{\Delta}_f < \\ \frac{\bar{\Delta}_\tau(1 + l_v)}{k_{\min} - l_\omega} + \bar{\Delta}_f < \delta_R \end{aligned}$$

where δ_R is defined in Proposition 5. For $0 < t \le T_1$, all signals are uniformly continuous; thus they are bounded. For $t > T_1$, $\|\bar{\boldsymbol{R}}_{3e}\| + \|\boldsymbol{\Delta}_f\| < \delta_R$, because of the ultimate boundedness of $\bar{\boldsymbol{R}}_{3e}$. According to Proposition 5, $|\phi| < U_\phi$ and $|\theta| < U_\theta$ are established for $t > T_1$, and 2) is proved.

All requirements of Proposition 5 are then satisfied, so that planar tracking error $\bar{\boldsymbol{p}}_e$ is ultimately bounded. Requirements of Proposition 4 are assured by the boundedness of ϕ and θ, and the altitude tracking error z_e can also be proved ultimately bounded. This proves 3). □

5 Simulation and discussion

In the simulation, we use the un-simplified model (5)∼(8), with the forces and torques given by (9) and (10). Parameters of the autonomous helicopter are cited from [27]. The constraints of the main rotor thrust and fuselage attitude are given in Table 1.

The reference trajectory to be tracked is given by

$$\begin{aligned} x_r(t) &= 9.6 \times 10^{-8}t^5 - 1.12 \times 10^{-5}t^4 + 3.2 \times 10^{-4}t^3 + 0.2 \\ y_r(t) &= -5.76 \times 10^{-8}t^5 + 6.4 \times 10^{-6}t^4 - 1.6 \times 10^{-4}t^3 - 0.2 \\ z_r(t) &= 1.152 \times 10^{-7}t^5 - 1.44 \times 10^{-5}t^4 + 4.8 \times 10^{-4}t^3 \\ \psi_r(t) &= \mathrm{atan2}(\dot{y}_r, \dot{x}_r) \end{aligned}$$

The initial position and velocity are supposed to be $\boldsymbol{p}_0 = [4, 5, 2]^{\mathrm{T}}$(m) and $\boldsymbol{v}_0 = [0.2, -0.2, 0]^{\mathrm{T}}$, respectively. The initial yaw angle is supposed to be $\psi_0 = 1$ rad. The initial values of other states are supposed to be zeros.

The bounds of the second-order derivatives of the reference trajectory are calculated by

$$|\ddot{z}_r| \le 0.015,\ \|\ddot{\bar{\boldsymbol{p}}}_r\| \le 0.03 \tag{57}$$

The expected values of U_ϕ and U_θ suggest that $M_R = 2.7$ in Proposition 5. Substituting (27) into (26) and (31) yields the available ranges of the control parameters

$$|k_z| + |k_w| < 1.9,\ |k_p| + |k_v| < 1.9$$

The values of control parameters are listed in Table 2.

Table 1 Constraints of thrust and attitude

Constraint	Value	Constraint	Value
U_t	68.6 N	U_T	102.9 N
U_ϕ	0.34 rad	U_θ	0.34 rad

Table 2 Control parameters

Parameter	Value	Parameter	Value
k_z	1	k_w	0.5
k_p	1.2	k_v	0.4
$k_{\gamma p}$	2.12	$k_{\gamma i}$	2.25
$k_{\psi p}$	0.35	$k_{\psi i}$	0.06
$k_{\omega p}$	5	$k_{\omega i}$	12.96

The simulation results are displayed in Figs. 2∼6. As can be seen from Figs. 2 and 3, the closed-loop system tracks the reference trajectory with ultimately bounded static errors. In the static state, the relatively large value of y_e is due to the disturbance resulted from the tail rotor thrust. Fig. 4 demonstrates that the attitude of the fuselage is maintained in secure ranges, with magnitudes of roll and pitch angles less than 0.17 rad, or 10 deg. Besides, the tracking performance of the yaw angle is satisfactory. The main rotor thrust and the corresponding main rotor collective pitch are displayed in Fig. 5, where the main rotor thrust is smooth and bounded within small ranges, indicating that the saturated control is effective. Although no explicit constraints are assigned directly for the collective

pitch of the tail rotor (T_t) and cyclic pitches of the main rotors (a_s and b_s), their actual values are bounded with small ranges (less than 0.17 rad, or 10 deg), as are shown in Fig. 6. In summary, the simulation results demonstrate that under the proposed partially saturated controller, the tracking errors are ultimately bounded, while the main rotor thrust and fuselage attitude satisfy the predefined constraints.

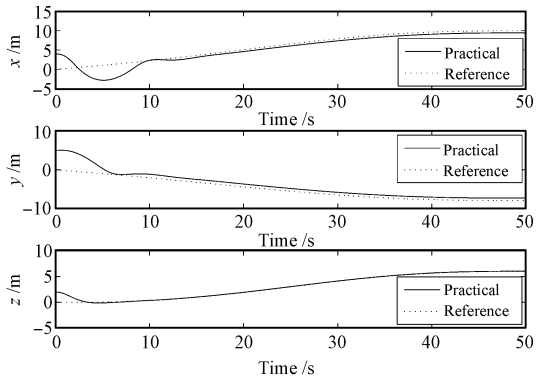

Fig. 2 The position of the closed-loop system (The actual position tracks the reference position.)

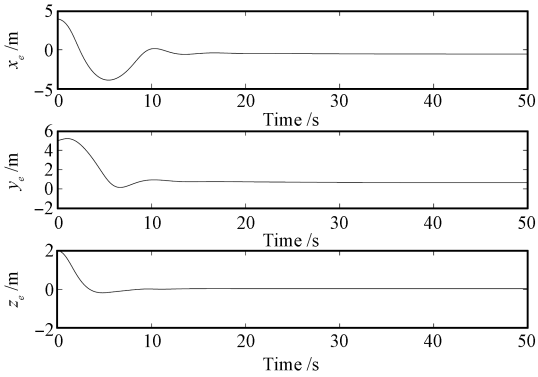

Fig. 3 Tracking errors of the closed-loop system (Tracking errors are ultimately bounded.)

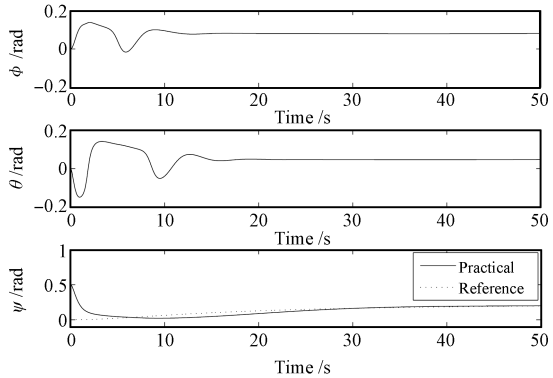

Fig. 4 The attitude of the closed-loop system (Roll and pitch angles are maintained very small, while the yaw angle tracks its reference signal.)

To better evaluate the proposed controller, the simulation results of a closed-loop system with non-saturated control are provided in Figs. 7 ∼ 9. The non-saturated control is designed by using the backstepping approach, with control parameters selected similar to those of the proposed saturated control. As can be seen from Fig. 7, the non-saturated control seems superior in transient performances of tracking errors. However, Fig. 8 indicates that the attitude of the closed-loop system with non-saturated control is somewhat dangerous, since the roll and pitch angles reach some excessively large values. In Fig. 9, it is obvious that the main rotor thrust varies sharply, which is certainly undesirable.

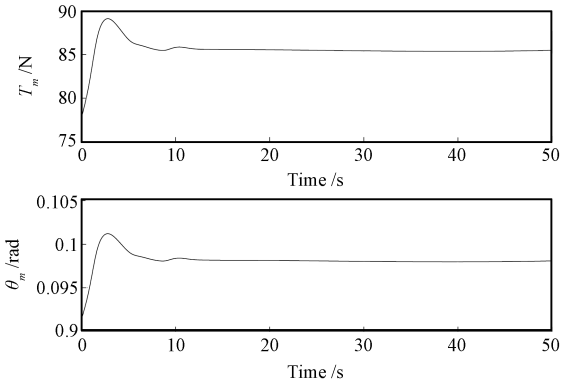

Fig. 5 The main rotor thrust and the main collective pitch of closed-loop system (They satisfy the predefined constraints.)

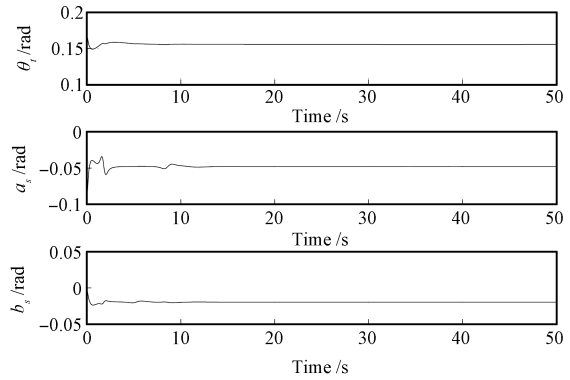

Fig. 6 Collective pitch of the tail rotor, and cyclic pitches of the main rotor (Their values are within small ranges (less than 10 deg).)

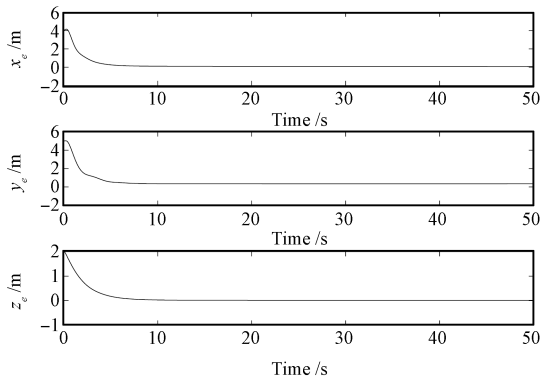

Fig. 7 Tracking errors of the closed-loop system without saturated control (Transient performances are better.)

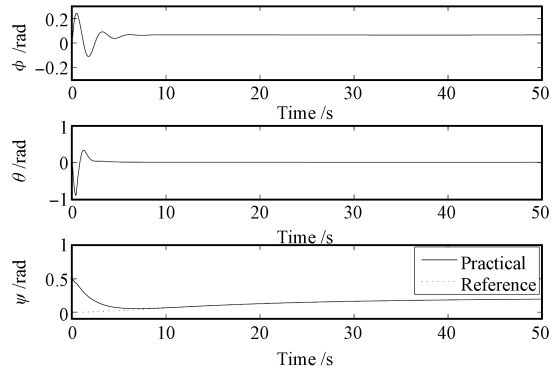

Fig. 8 The attitude of the closed-loop system without saturated control (Roll and pitch angles might reach excessively large values.)

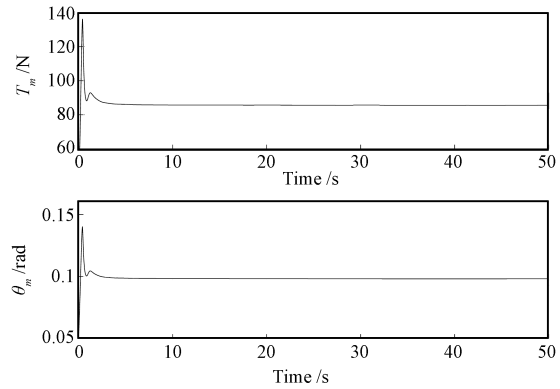

Fig. 9 The main rotor thrust and the main collective pitch of closed-loop system without saturated control (They vary sharply.)

6 Conclusion

A nonlinear controller is proposed to achieve the trajectory tracking of a 6-DOF model-scaled helicopter in the presence of constraints on the main rotor thrust and fuselage attitude. With some extensions, the technique for the saturated control of a 3-DOF VTOL aircraft is adopted as the basic methodology in this research. Instead of the traditional un-smooth saturation function, the smooth hyperbolic tangent function is employed as the saturation function, such that the derivatives of virtual control are possible to be solved analytically, and the Barbalat Lemma can be applied to stability analysis. The simulation results demonstrate that under the proposed partially saturated controller, tracking errors are ultimately bounded while constraints on the main rotor thrust and fuselage attitude are satisfied.

Appendix

The hyperbolic function $\tanh(\cdot)$ in (1) possesses the following superior properties.

Property A1. $\tanh(s)$ is differentiable for $s \in \mathbf{R}$, and
1) $-1 < \tanh(s) < 1$;
2) $s\tanh(s) > 0$, $\forall s \neq 0$; $s\tanh(s) = 0 \Leftrightarrow s = 0$.

Property A2. The 1st-order and 2nd-order derivatives of the hyperbolic tangent function are bounded, namely

$$0 < \frac{\mathrm{d}\tanh(s)}{\mathrm{d}s} = \frac{4}{(\mathrm{e}^s + \mathrm{e}^{-s})^2} \leq 1 \tag{A1}$$

$$-0.77 < \frac{\mathrm{d}^2\tanh(s)}{\mathrm{d}s^2} = \frac{-8(\mathrm{e}^s - \mathrm{e}^{-s})}{(\mathrm{e}^s + \mathrm{e}^{-s})^3} < 0.77 \tag{A2}$$

Property A3. Given any interval $D_1 : \{s \mid |s| < \bar{s}, \bar{s} > 0\}$, there always exists a positive number $\chi(\bar{s})$ such that $\chi(\bar{s})|s| \leq |\tanh(s)| \leq |s|$.

The results of Property A1 and Property A2 are intuitive. In Property A3, $|\tanh(s)| \leq |s|$ can be proved directly by considering (A1) and $\tanh(0) = 0$; and $\chi(\bar{s})|s| \leq |\tanh(s)|$ can be proved by selecting

$$0 < \chi(\bar{s}) < \frac{1}{\bar{s}}\tanh(\bar{s}) \tag{A3}$$

Property A4. For any vector $\boldsymbol{x} = [x_1, \cdots, x_n]^{\mathrm{T}} \neq 0$,

$$\boldsymbol{x}^{\mathrm{T}}\tanh(\boldsymbol{x}) = \sum_{i=1}^{n} x_i \tanh(x_i) > 0$$

Property A5. Given a region

$$D_2 : \{\boldsymbol{x} \in \mathbf{R}^n \mid \|\boldsymbol{x}\| < \bar{x}, \bar{x} > 0\}$$

there always exists a positive number $\chi(\bar{x})$ such that $\chi(\bar{x})\|\boldsymbol{x}\| \leq \|\tanh(\boldsymbol{x})\| \leq \|\boldsymbol{x}\|$.

The result of Property A4 is intuitive. Property A5 is a vector form of Property A3, and can be proved similarly.

Definition A1. The square of a vector $\boldsymbol{x} = [x_1, \cdots, x_n]^{\mathrm{T}}$ is defined by $\boldsymbol{x}^2 := [x_1^2, \cdots, x_n^2]^{\mathrm{T}}$.

Definition A2. The kth-order ($k = 1, 2, \cdots$) derivative of the vector hyperbolic function is

$$\frac{\mathrm{d}^k\tanh(\boldsymbol{x})}{\mathrm{d}\boldsymbol{x}^k} := \begin{bmatrix} \frac{\mathrm{d}^k\tanh(x_1)}{\mathrm{d}x_1^k} & 0 & 0 \\ \vdots & \vdots & \vdots \\ 0 & 0 & \frac{\mathrm{d}^k\tanh(x_n)}{\mathrm{d}x_n^k} \end{bmatrix}$$

where $\boldsymbol{x} = [x_1, \cdots, x_n]^{\mathrm{T}}$.

It follows from Definitions 1, A1 $\sim$ A2 that

$$\frac{\mathrm{d}\tanh(\boldsymbol{x})}{\mathrm{d}t} = \begin{bmatrix} \frac{\mathrm{d}\tanh(x_1)}{\mathrm{d}x_1}\dot{x}_1 \\ \vdots \\ \frac{\mathrm{d}\tanh(x_n)}{\mathrm{d}x_n}\dot{x}_n \end{bmatrix} = \begin{bmatrix} \frac{\mathrm{d}\tanh(x_1)}{\mathrm{d}x_1} & 0 & 0 \\ \vdots & \vdots & \vdots \\ 0 & 0 & \frac{\mathrm{d}\tanh(x_n)}{\mathrm{d}x_n} \end{bmatrix} \begin{bmatrix} \dot{x}_1 \\ \vdots \\ \dot{x}_n \end{bmatrix} = \frac{\mathrm{d}\tanh(\boldsymbol{x})}{\mathrm{d}\boldsymbol{x}}\dot{\boldsymbol{x}}$$

$$\frac{\mathrm{d}^2\tanh(\boldsymbol{x})}{\mathrm{d}t^2} = \frac{\mathrm{d}\tanh(\boldsymbol{x})}{\mathrm{d}\boldsymbol{x}}\ddot{\boldsymbol{x}} + \frac{\mathrm{d}^2\tanh(\boldsymbol{x})}{\mathrm{d}\boldsymbol{x}^2}\dot{\boldsymbol{x}}^2$$

Definition A3. The vector integral is

$$\int_{\boldsymbol{z}}^{\boldsymbol{y}} \boldsymbol{x}^{\mathrm{T}}\mathrm{d}\boldsymbol{x} := \left[\int_{z_1}^{y_1} x_1\mathrm{d}x_1, \cdots, \int_{z_n}^{y_n} x_n\mathrm{d}x_n\right]^{\mathrm{T}}$$

where $\boldsymbol{x} = [x_1, \cdots, x_n]^{\mathrm{T}}$, $\boldsymbol{y} = [y_1, \cdots, y_n]^{\mathrm{T}}$ and $\boldsymbol{z} = [z_1, \cdots, z_n]^{\mathrm{T}}$.

With the above properties and definitions, proofs of Proposition 2 and Proposition 3 can be given as follows.

Proof of Proposition 2. Define the Lyapunov candidate as

$$L_0 = \alpha \int_0^{k\boldsymbol{\xi}_1+l\boldsymbol{\xi}_2} \tanh(\boldsymbol{\xi})^{\mathrm{T}} \mathrm{d}\boldsymbol{\xi} + \beta \int_0^{l\boldsymbol{\xi}_2} \tanh(\boldsymbol{\xi})^{\mathrm{T}} \mathrm{d}\boldsymbol{\xi} + \frac{k}{2}\boldsymbol{\xi}_2^{\mathrm{T}}\boldsymbol{\xi}_2 > 0$$

Its time derivative is

$$\dot{L}_0 = \alpha \tanh(k\boldsymbol{\xi}_1 + l\boldsymbol{\xi}_2)^{\mathrm{T}}(k\dot{\boldsymbol{\xi}}_1 + l\dot{\boldsymbol{\xi}}_2) + \beta l \tanh(l\boldsymbol{\xi}_2)^{\mathrm{T}}\dot{\boldsymbol{\xi}}_2 + k\boldsymbol{\xi}_2^{\mathrm{T}}\dot{\boldsymbol{\xi}}_2 = -l\theta^{\mathrm{T}}\theta - \beta k \boldsymbol{\xi}_2^{\mathrm{T}} \tanh(l\boldsymbol{\xi}_2) < 0$$

where $\boldsymbol{\theta} := \alpha \tanh(k\boldsymbol{\xi}_1 + l\boldsymbol{\xi}_2) + \beta \tanh(l\boldsymbol{\xi}_2)$. As a result, the global asymptotical stability is proved.

Let $\boldsymbol{\mu}_1 = k\boldsymbol{\xi}_1 + l\boldsymbol{\xi}_2$, $\boldsymbol{\mu}_2 = l\boldsymbol{\xi}_2$ and $\boldsymbol{\mu} = [\boldsymbol{\mu}_1^{\mathrm{T}}, \boldsymbol{\mu}_2^{\mathrm{T}}]^{\mathrm{T}}$, and select a region:

$$D_3 : \{\boldsymbol{\mu} \mid \|\boldsymbol{\mu}\| < \bar{\mu}, \bar{\mu} > 0\} \tag{A4}$$

According to Property 5, there always exists a positive number $\chi(\bar{\mu})$ satisfying $\chi\|\boldsymbol{\mu}\| < \|\tanh(\boldsymbol{\mu})\| < \|\boldsymbol{\mu}\|$, such that

$$L_0 > \frac{1}{2}\chi(\alpha\boldsymbol{\mu}_1^{\mathrm{T}}\boldsymbol{\mu}_1 + \beta\boldsymbol{\mu}_2^{\mathrm{T}}\boldsymbol{\mu}_2) + \frac{k}{2l^2}\boldsymbol{\mu}_2^{\mathrm{T}}\boldsymbol{\mu}_2 = \frac{1}{2}\boldsymbol{\mu}^{\mathrm{T}} \begin{bmatrix} \chi\alpha I_{n\times n} & 0 \\ 0 & (\chi\beta + \frac{k}{l^2})I_{n\times n} \end{bmatrix} \boldsymbol{\mu} > \chi_1\|\boldsymbol{\mu}\|^2 \tag{A5}$$

where $\chi_1 = \min\left[\frac{1}{2}\chi\alpha, \frac{1}{2}\left(\chi\beta + \frac{k}{l^2}\right)\right]$. Moreover,

$$\dot{L}_0 < -l\boldsymbol{\theta}^{\mathrm{T}}\boldsymbol{\theta} - \frac{k\beta}{l}\tanh(\boldsymbol{\mu}_2)^{\mathrm{T}}\tanh(\boldsymbol{\mu}_2) = -\tanh(\boldsymbol{\mu})^{\mathrm{T}} \begin{bmatrix} \alpha^2 l I_{n\times n} & \alpha\beta l I_{n\times n} \\ \alpha\beta l I_{n\times n} & (\beta^2 l + \frac{k\beta}{l})I_{n\times n} \end{bmatrix} \tanh(\boldsymbol{\mu}) = -\tanh(\boldsymbol{\mu})^{\mathrm{T}} D \tanh(\boldsymbol{\mu})$$

The symmetric matrix D is positive definite, because there exists an invertible matrix

$$T = \begin{bmatrix} I_{n\times n} & -\frac{\beta}{\alpha}I_{n\times n} \\ 0 & I_{n\times n} \end{bmatrix}$$

such that

$$T^{\mathrm{T}}DT = \begin{bmatrix} \alpha^2 l I_{n\times n} & 0 \\ 0 & \frac{k\beta}{l}I_{n\times n} \end{bmatrix}$$

Its eigenvalues are positive. With Property 3,

$$\dot{L}_0 < -\chi_2\|\boldsymbol{\mu}\|^2 \tag{A6}$$

where

$$\chi_2 = \min\left[\alpha^2 l\chi^2, \frac{k\beta}{l}\chi^2\right] \tag{A7}$$

indicating that system (3) is semi-globally exponentially stable in the region of D_3 given by (A4), where bound $\bar{\mu}$ can be selected arbitrarily large. □

Remark A1. A large $\bar{\mu}$ results in a small $\chi(\bar{\mu})$, leading to small χ_1 and χ_2. Since χ_2 is proportional to the converging rate, as is shown by (A6), the exponential stability of system (3) reduces to asymptotical stability as the region $\{\boldsymbol{\mu} \mid \|\boldsymbol{\mu}\| < \bar{\mu}, \bar{\mu} > 0\}$ increases.

Proof of Proposition 3. Use L_0 as the Lyapunov candidate.

$$\dot{L}_0 < -\chi_2\|\boldsymbol{\mu}\|^2 + \alpha l\bar{\Delta}\|\boldsymbol{\mu}_1\| + \beta l\bar{\Delta}\|\boldsymbol{\mu}_2\| + \frac{k}{l}\bar{\Delta}\|\boldsymbol{\mu}_2\| < -\chi_2\|\boldsymbol{\mu}\|^2 + \chi_3\bar{\Delta}\|\boldsymbol{\mu}\|$$

where $\chi_3 = \max\left[\alpha l, \left(\beta l + \frac{k}{l}\right)\right]$. Therefore, $\boldsymbol{\mu}$ converges into

$$D_4 : \left\{\boldsymbol{\mu} \,\middle|\, \|\boldsymbol{\mu}\| < \frac{\chi_3}{\chi_2}\bar{\Delta}\right\}$$

To guarantee that $\|\boldsymbol{\mu}\| < \bar{\mu}$, $\bar{\Delta}$ should satisfy

$$\frac{\chi_3}{\chi_2}\bar{\Delta} < \bar{\mu} \;\Leftrightarrow\; \max\left[\alpha l\bar{\Delta}, \left(\beta l + \frac{k}{l}\right)\bar{\Delta}\right] < \bar{\mu}\chi_2 \;\Leftrightarrow\; \bar{\Delta} < \min\left[\frac{\bar{\mu}\chi_2}{\alpha l}, \frac{\bar{\mu}\chi_2}{(\beta l + \frac{k}{l})}, \alpha + \beta\right] \tag{A8}$$

where χ_2 is given by (A7). □

References

1 Shakernia O, Ma Y, Koo T J, Sastry S. Landing an unmanned air vehicle: vision based motion estimation and nonlinear control. *Asian Journal of Control*, 1999, **1**(3): 128−145

2 Koo T J, Sastry S. Output tracking control design of a helicopter model based on approximate linearization. In: Proceedings of the 37th IEEE Conference on Decision and Control. Tempa, USA, 1998. 3635−3640

3 Raptis I A, Valavanis K P, Vachtsevanos G J. Linear tracking control for small-scale unmanned helicopters. *IEEE Transactions on Control Systems Technology*, 2012, **20**(4): 995−1010

4 Raptis I A, Valavanis K P, Moreno W A. A novel nonlinear backstepping controller design for helicopters using the rotation matrix. *IEEE Transactions on Control Systems Technology*, 2011, **19**(2): 465−473

5 Zhu B, Huo W. Robust nonlinear control for a model-scaled helicopter with parameter uncertainties. *Nonlinear Dynamics*, 2013, **73**(1−2): 1139−1154

6 He Y Q, Han J D. Acceleration feedback enhanced H_∞ disturbance attenuation control for a class of nonlinear underactuated vehicle systems. *Acta Automatica Sinica*, 2008, **34**(5): 558−564

7 Gadewadikar J, Lewis F, Subbarao K, Chen B M. Structured H-infinity command and control-loop design for unmanned helicopters. *Journal of Guidance, Control, and Dynamics*, 2008, **31**(4): 1093−1102

8 Cai G W, Chen B M, Dong X X, Lee T H. Design and implementation of a robust and nonlinear flight control system for an unmanned helicopter. *Mechatronics*, 2011, **21**(5): 803−820

9 Liu C J, Chen W H, Andrews J. Tracking control of small-scale helicopters using explicit nonlinear MPC augmented with disturbance observers. *Control Engineering Practice*, 2012, **20**(3): 258−268

10 Marchand N, Hably A. Global stabilization of multiple integrators with bounded controls. *Automatica*, 2005, **41**(12): 2147−2152

11 Saberi A, Lin Z, Teel A R. Control of linear systems with saturating actuators. *IEEE Transactions on Automatic Control*, 1996, **41**(3): 368−378

12 Sussman H J, Sontag E D, Yang Y. A general result on the stabilization of linear systems using bounded controls. *IEEE Transactions on Automatic Control*, 1994, **39**(12): 2411−2425

13 Teel A R. Global stabilization and restricted tracking for multiple integrators with bounded controls. *Systems & Control Letters*, 1992, **18**(3): 165−171

14 Wang Y, Ma R N. Global stabilization of feedforward nonlinear system based on nested saturated control. *Acta Automatica Sinica*, 2010, **36**(4): 528−533

15 Zhou J, Wen C Y. *Adaptive Backstepping Control of Uncertain Systems*. Berlin: Springer-Verlag, 2008. 189−197

16 Mazenc F, Iggidr A. Backstepping with bounded feedbacks. *Systems and Control Letters*, 2004, **51**(3−4): 235−245

17 Teel A R. A nonlinear small gain theorem for the analysis of control systems with saturation. *IEEE Transactions on Automatic Control*, 1996, **41**(9): 1256−1270

18 Ailon A. Simple tracking controllers for autonomous VTOL aircraft with bounded inputs. *IEEE Transactions on Automatic Control*, 2010, **55**(3): 737−743

19 Olfati-Saber R. Global configuration stabilization for the VTOL aircraft with strong input coupling. *IEEE Transactions on Automatic Control*, 2002, **47**(11): 1949−1952

20 Hong Y, Yao B. A globally stable saturated desired compensation adaptive robust control for linear motor systems with comparative experiments. *Automatica*, 2007, **43**(10): 1840−1848

21 Wang J J, Liu D L, Wang B J. Research on one type of saturated nonlinear stabilization control method of X-Z inverted pendulum. *Acta Automatica Sinica*, 2013, **39**(1): 92−96

22 Isidori A, Marconi L, Serrani A. Robust nonlinear motion control of a helicopter. *IEEE Transactions on Automatic Control*, 2003, **48**(3): 413−426

23 Marconi L, Naldi R. Robust full degree-of-freedom tracking control of a helicopter. *Automatica*, 2007, **43**(11): 1909−1920

24 Sontag E D, Wang Y. New characterizations of input-to-state stability. *IEEE Transactions on Automatic Control*, 1996, **41**(9): 1283−1294

25 Zhu B, Huo W. 3-D path-following control for a model-scaled autonomous helicopter. *IEEE Transactions on Control Systems Technology*, 2014, **22**(5): 1927−1934

26 Bramwell A R S, Done G, Balmford D. *Bramwell's Helicopter Dynamics* (Second Edition). Butterworth Heinmann, 2001. 48−51

27 Gavrilets V. Autonomous Aerobatic Maneuvering of Miniature Helicopter [Ph. D. dissertation], Massachusetts Institute of Technology, 2003.

ZHU Bing Postdoctor at University of Pretoria. He received his Ph. D. degree in control theory and control engineering from Beihang University in 2013. His research interest covers helicopter flight control, model predictive control and its application to new energy systems. Corresponding author of this paper.
E-mail: bing.zhu@up.ac.za

HUO Wei Professor at Beihang University. He received his Ph. D. degree in control theory and application from Beihang University in 1990. His research interest covers nonlinear control, robotics, and helicopter flight control.
E-mail: weihuo@buaa.edu.cn